Energy & Environmental Science

Rewiring photosynthesis: a Photosystem I-hydrogenase chimera that makes H_2 in vivo

Journal:	*Energy & Environmental Science*
Manuscript ID	EE-ART-11-2019-003859.R2
Article Type:	Paper
Date Submitted by the Author:	06-Apr-2020
Complete List of Authors:	Kanygin, Andrey; Arizona State University, Molecular Sciences Milrad, Yuval; Tel Aviv University, Plant Sciences and Food Security Thummala, Chandrasekhar; Yogi Vemana University, Environmental Science; Yogi Vemana University, Environmental Science Reifschneider, Kiera; Arizona State University Baker, Patricia; Arizona State University, Molecular Sciences Marcu, Pini; Tel Aviv University, Molecular Biology & Ecology of Plants Yacoby, Iftach; Tel Aviv University, Plant sciences Redding, Kevin; Arizona State University, Chemistry & Biochemistry

Rewiring photosynthesis: a Photosystem I-hydrogenase chimera that makes H_2 *in vivo*

Received 00th January 20xx,
Accepted 00th January 20xx

DOI:

Andrey Kanygin[a], Yuval Milrad[b], Chandrasekhar Thummala[a,c], Kiera Reifschneider[a†], Patricia Baker[a], Pini Marco[b], Iftach Yacoby[b*] and Kevin E. Redding[a*]

Harnessing the power of photosynthesis to catalyze novel light-driven redox chemistry requires a way to intercept electron flow directly from the photosynthetic electron transport chain (PETC). As a proof of concept, an *in vivo* fusion of Photosystem I (PSI) and algal hydrogenase was created by insertion of the HydA sequence into the PsaC subunit. The PSI and hydrogenase portions are co-assembled and active *in vivo*, effectively creating a new photosystem. Cells expressing only the PSI-hydrogenase chimera make hydrogen at high rates in a light-dependent fashion for several days. In these engineered cells, photosynthetic electron flow is directed away from CO_2 fixation and towards proton reduction, demonstrating the possibility of driving novel redox chemistries using electrons from water splitting and the photosynthetic electron transport chain.

Broader context

Re-engineering fundamental processes in photosynthetic microorganisms offers a cheap and renewable platform for creating bio-factories capable of driving difficult redox transformations, powered only by the sun and using water as the electron source. To maximize the usefulness of such engineered systems, we require a way to intercept intracellular electron flow at the most reductive potential. We have taken the approach of positioning redox enzymes to directly capture electrons from Photosystem I (PSI) before they enter the general cellular pool. In this paper, we describe a functional fusion of PSI with the hydrogenase enzyme to re-direct electrons from carbon fixation to proton reduction. This results in a large fraction of the electrons from water oxidation by Photosystem II being used to make dihydrogen. Perhaps most importantly, we have identified a site in PSI where redox enzymes can be attached to intercept electrons from the photosynthetic electron transport chain.

Introduction

Conversion of algal cells into solar-powered biofactories generating high-energy product molecules is a promising avenue for addressing the ever-increasing global energy demand, due to its environmental friendliness and cheap replication. Hydrogen (H_2) is an attractive target product for several reasons. It is an important commodity with over 60 million tons produced globally, but ~95% of it is produced from steam reformation of fossil fuels, thus contributing to the rise of atmospheric CO_2.[1] The [FeFe] hydrogenase enzyme catalyzes the rapid and reversible reduction of protons ($2\ H^+ + 2\ e^- \leftrightarrows H_2$). The active site of the enzyme is a metallic cofactor that is O_2-sensitive and must be inserted by maturation factors.[2] These characteristics are shared with many important redox enzymes, making hydrogenase an ideal test case for synthetic biology manipulations.

In the thylakoid membranes of the chloroplast, the photosynthetic electron transport chain (PETC) performs light-driven electron transport from water to ferredoxin (Fd) and pumps protons across the membrane, ultimately providing metabolic energy (ATP) and low-potential reductant (NADPH) to drive CO_2 fixation by the Calvin-Benson-Bassham (CBB) cycle (**Fig. 1A**).[3] Algal hydrogenases are particularly attractive as producers of a solar fuel due to their structural simplicity (e.g., a single catalytic domain)[4] and ability to couple sunlight to hydrogen production by using reducing equivalents from the PETC. The active site of the enzyme consists of a [4Fe-4S] cluster coupled to a di-iron subsite containing CO and CN^- ligands; insertion of the latter requires three maturase proteins.[5] Algal hydrogenases normally function to dispose of excess reductant under anoxic conditions, to facilitate fermentative processes in the dark or the initiation of photosynthetic linear electron flow during dark-to-light transitions.[6] Despite various attempts to improve hydrogen production in green algae, it has not yet become economically feasible due primarily to two major issues: inactivation of the hydrogenase by oxygen and competition for reductant with other processes.[7,8]

It has recently been shown that algal hydrogenases compete poorly for reduced Fd.[9] The primary competitor, Fd:$NADP^+$ oxidoreductase (FNR), not only has a cellular abundance ~70 times that of hydrogenase,[10] but it also has a higher affinity for Fd (K_m = 0.8-2.6 μM)[11,12] than does hydrogenase (K_m = 3.4-35 μM)[13–15]. As the estimated Fd concentration in the chloroplast is ~120 μM^+, both enzymes should be operating near saturation when the Fd pool is mostly reduced. Thus, the competition between them should be largely dependent on the concentrations and k_{cat} values of the respective enzymes, and one would predict that roughly 14 times as many electrons would be used to reduce $NADP^+$ via FNR than to reduce protons via hydrogenase[†]. Thus, it is unsurprising that H_2 production in algae decreases upon activation of the CBB cycle.[16,17]

[a] *School of Molecular Sciences and Center for Bioenergy & Photosynthesis, Arizona State University, Tempe, Arizona, USA.*
[b] *School of Plant Sciences and Food Security, Tel Aviv University, Tel Aviv, Israel.*
[c] *Department of Environmental Science, Yogi Vemana University, Kadapa, Andhra Pradesh, India.*
† Current address: 3582 AB Utrecht, Netherlands.
*Corresponding authors.
Email: kredding@asu.edu ORCID:0000-0003-2819-4022 and Iftachy@tauex.tau.ac.il
ORCID: 0000-0003-0177-0624
Electronic Supplementary Information (ESI) available: [details of any supplementary information available should be included here]. See DOI: 10.1039/x0xx00000x

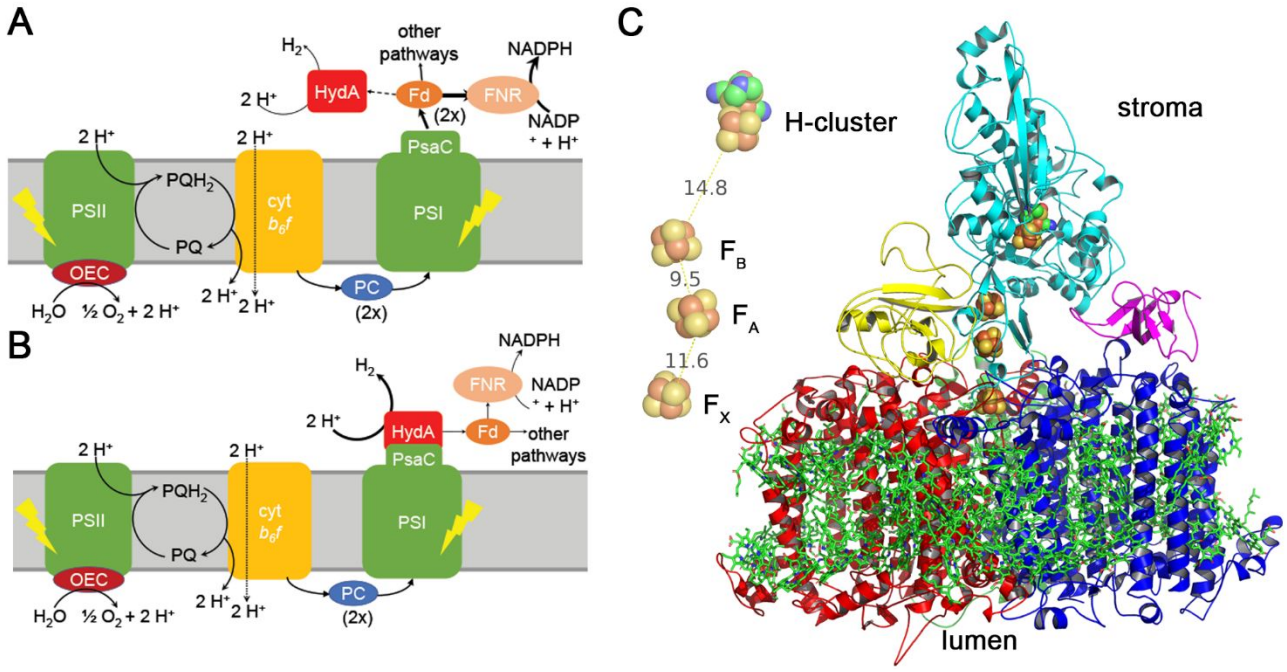

Fig. 1 The photosynthetic electron transport chain (PETC) in WT cells **(A)**, the proposed system **(B)**, and a model of PSI-HydA **(C)**. **(A)** The PETC in the thylakoid membrane drives linear electron flow, with water being oxidized by the oxygen evolving complex (OEC) of PSII and Fd being reduced by PSI, accompanied by formation of proton motive force. Two electrons will exit the PETC for each H_2O oxidized. Under most conditions, NADPH is the major product, made by FNR. H_2 is a minor and/or transient product under anoxic conditions. **(B)** In the system described here, hydrogenase (HydA) is directly attached to PSI, which should direct most electrons to H_2 production at the expense of Fd reduction. **(C)** A model of PSI core subunits (PsaA – red, PsaB – blue) as ribbon diagrams, with PsaC-HydA2 (cyan), PsaD (yellow) and PsaE (magenta). Antenna pigments (chlorophyll (Chl) a and β-carotenes) are shown as green stick models, while FeS clusters and the H-cluster are shown as space-filling models. The predicted edge-to-edge distances between the inorganic substituents of the FeS clusters and the H-cluster (in Å) are shown to the left of the model.

In order to circumvent this problem, we sought a way to divert electrons from the PETC towards H_2 production. PSI is the ideal choice for the diversion point for several reasons. The terminal cofactors of PSI are at a very low potential (-450/-490 mV vs. SHE),[18] thus maximizing the driving force of the engineered redox chemistry. In addition, allowing electrons originating from water oxidation by PSII to transit the PETC maximizes the proton pumping carried out by the PETC, and thereby ATP production by the thylakoid, thus maintaining viability of the cellular bio-factory. Diversion at an earlier point would diminish this advantage, while diversion after PSI would be much less effective – once electrons enter the Fd and NADPH pools, many metabolic processes can draw upon them.

Using a unicellular green alga (*Chlamydomonas reinhardtii*) as an experimental system, we created an *in vivo* fusion of PSI and the [FeFe] hydrogenase expressed by the organism (see **Fig. 1B**). While the structural gene for this hydrogenase is in the nuclear genome[19] and the core photosystem subunits are chloroplast encoded, it has been shown that active hydrogenase can be made from a gene transplanted into the chloroplast chromosome.[20,21] We show that photosynthetic flow in the re-engineered chloroplast is diverted from CO_2 fixation to proton reduction and results in sustained biohydrogen production.

Experimental

Chimeric protein design and homology modeling

The site of insertion of the hydrogenase domain corresponds to residues 32-36 (DGCKA) of *C. reinhardtii* PsaC. Residue Asp32 was replaced with Gly for additional flexibility and residues Cys34 and Lys35 were replaced with "trimmed" HydA2 sequence, such that PsaC-Gly33 was connected directly to the N-terminus of mature HydA2 (Ala63) and the C-terminus of HydA2 (Gly500) was connected to PsaC-Ala36 (see **Fig. S1**). Trimming of the *HYDA2* sequence consisted of removal of the transit peptide from the N-terminus (first 62 residues) and the last 5 residues (which are not conserved) from the C-terminus. To model the structure of PSI-HydA, the protein structure prediction webtool Phyre2[22] (intensive algorithm) was used to model individual subunits of *C. reinhardtii* PSI (PsaA, PsaB, PsaC, PsaD, PsaE and PsaF) and HydA2, based on the sequences of the polypeptides from protein data bank. Following removal of residues D32-K35 of PsaC in Pymol, the docking of HydA2 was performed using the ClusPro2 [23] server with distance restraints of 10 Å, corresponding to the amino acid residues involved in the junctions in the chimeric protein (Trp31 of PsaC to the N-terminal Gly of the modified HydA2 and the C-terminal Gly of the modified HydA2 to Ala36 of PsaC). The most plausible model based on ClusPro2's energy minimization algorithm was chosen and, after formation of two peptide bonds between PsaC and HydA2, the connecting loops were allowed to relax, using the ModLoop server.[24] PsaD and then PsaE were then docked to the PsaC-HydA2 chimera with ClusPro2 as well.

Generation of cells expressing PSI-hydrogenase

The *psaC-hydA2* fusion sequence (see **Fig. S1**) was synthesized by Genscript (Piscataway, NJ USA) and inserted via flanking *Nde*I and *Bgl*II sites into the pBS-EP5.8 *aadA* vector [25] digested with *Nde*I and *Bgl*II. The resulting pAK10G plasmid neatly replaces

the *psaC* gene with the designed *psaC-hydA2* fusion gene. This plasmid was introduced into the *hydA* [26] and PBC4-2 strains of *C. reinhardtii* by particle-mediated transformation. The latter strain combines two mutations in the chloroplast genome: deletion of *psaC* [27] and the hexahistidine-tagged *psaA* exon 1.[28] The transformants were initially selected on TAP plates with 100 mg/L spectinomycin in the dark. Individual colonies were passaged alternately on plates containing 100 mg/L streptomycin or 300 mg/L spectinomycin in the dark and colony purified until they became homoplasmic, as determined by PCR (see method below). The amplified PCR products were verified by Sanger sequencing to ensure that no mutations in the introduced *psaC-hydA2* gene had arisen during the process. The same transformation and verification steps were performed on the strain expressing a hexahistidine-tagged (H_6) version of PSI.[29]

PCR analysis of algal transformants

PsaC-HydA2 detection PCR was performed with flanking primers (PsaC5': TAATATGGAGATGACATATTTAG and PsaC3': GATCTCACCAAGATACTCCC) as well as with gene-specific primers (PsaC5'int: TCAATGTGTACGTGCTTGTCC and PsaC3'int: ACAACGTTTGCAACCTACACA) on 100 ng of genomic DNA using MeanGreen 2x Taq DNA polymerase master mix (Syzygy Biotech). Reactions (50 µL) were cycled 35 times (95 °C for 15 s, 51 °C for 15 s, 72 °C for 90 s) using initial primer concentrations of 0.5 µM. To determine the limits of detection of the PCR for the *psaC* gene, test PCR templates were generated by diluting genomic DNA from the *hydA* strain (containing *psaC*) into genomic DNA from the *psaCΔ* mutant (lacking *psaC*)[27] at the same concentration, in order to emulate conditions of heteroplasmy (10%, 1% *psaC*) and homoplasmy (100%, 0% *psaC*).

Growth conditions

Unless otherwise specified, algae were grown in liquid Tris-acetate-phosphate (TAP) medium with revised mineral nutrient supplement[30] in Erlenmeyer baffled cell-culture flasks under low ambient light conditions (~5 µmol photons m^{-2} s^{-1} PAR) with agitation (150 rpm). Larger cultures (1 L and greater) were grown with continuous stirring and sparging with sterile filtered air. For autotrophic growth, Tris-bicarbonate phosphate (TBP) medium was prepared by substituting 25 mM sodium bicarbonate (pH 7.0) for acetate (~16.6 mM) in the medium.

An FMT-150 (Photon Systems International, Brno, Czech Republic) photobioreactor (PBR) system equipped with pH and Clark-type O_2 electrodes was used to obtain growth curves at constant temperature (24 °C). Starter cultures were pre-grown in TAP and washed twice with TBP. Cells were resuspended in TBP to a final OD_{680} of 0.1. At the beginning of each run, the photobioreactor vessel was sparged with N_2 for ~1 hour. Afterwards, the cultures were sealed and stirred for the duration of the experiment.

Chlorophyll (Chl) measurement

Concentrations of Chl *a* and *b* were determined as described in Porra et al.[31]

Thylakoid and PSI preparation

Thylakoid membranes were prepared as previously described,[25] with minor modifications outlined below. Cells were grown in 4-L flasks and centrifuged at 3500 x *g* at 4 °C for 10 min. The pellet was washed with H1 buffer (25 mM HEPES-KOH, 5 mM $MgCl_2$, 0.3 M sucrose, pH 7.5), flash-frozen in liquid nitrogen, and stored at –80 °C. Subsequent steps were performed in the dark and samples were kept at 4 °C. Cells were resuspended at 2-4 $x10^8$ cells mL^{-1} in H1 containing 1 mM phenylmethane sulfonyl fluoride to inhibit proteolysis. Cell breakage was accomplished with a French Press (Aminco) at ~1.7 tons pressure. Unbroken cells were pelleted by centrifugation at 2000 *x g* for 1 min, and the supernatant was centrifuged at 20000 *x g* for 10 min. The pelleted membranes were washed in 50 mL of H2 buffer (5 mM HEPES-KOH, 10 mM EDTA, 0.3 M sucrose pH 7.5) and resuspended in H3 buffer (5 mM HEPES-KOH, 10 mM EDTA, 1.8 M sucrose, pH 7.5). A discontinuous sucrose gradient was prepared using H3 buffer containing suspended thylakoid membranes, which was in turn overlaid with 1.3 M sucrose and 0.5 M sucrose solutions. After 1 hour of centrifugation in an SW-28 rotor at 25,000 rpm, the upper green band (0.5/1.3 M interface) was collected and washed with 3x volume of H6 buffer (5 mM HEPES-KOH, 10 mM EDTA pH 7.5). Purified thylakoids were concentrated by centrifugation (90,000 x *g* for 30 min) and resuspended in H6 + 20% glycerol and were either stored at 200 K after flash-freezing in liquid N_2 or solubilized for PSI purification.

PSI particles were purified from thylakoid membranes on sucrose gradients after solubilization with β-dodecyl maltoside (β-DDM), as described in Li et al.[29] Purification of hexahistidine-tagged PSI was performed as described previously,[28] except that a Ni(II)-iminodiacetic acid (IDA) resin (G-biosciences, St. Louis, MO U.S.A.) was used.

Anoxic PSI-HydA2 isolation

Twelve liters of cells grown aerobically in TAP to mid-log phase were harvested and resuspended in fresh TAP to ~200-300 µg/mL of total Chl and sparged with Ar for ~ 4 h. After this point, all preparation steps were done in an anaerobic glovebox (Coy) filled with a 5% H_2/95% N_2 gas mixture. Sodium dithionite was added to 2mM final concentration and 5-mL aliquots were pelleted and stored in liquid nitrogen. Once thawed, each pellet was resuspended in breaking buffer (0.1 M Tris-HCl, pH 8.0), 10 mM EDTA-KOH, 1 mM PMSF and 2 mM $Na_2S_2O_4$) in a total volume of 30 mL. Cell lysis was accomplished using a Branson sonifier S-450 operated at amplitude 3, 50% duty cycle for a total of 6 min (2 minutes sonication followed by 2 min waiting) on chilled beads (-20 to -10 °C) to achieve complete cell lysis. Crude thylakoids were pelleted (208,000 xg, 15 min, 4 °C), and resuspended in solubilization buffer (25 mM Tricine-KOH, pH 8.0, 300 mM KCl, 10% glycerol) containing 2 mM sodium dithionite. Solubilization and IMAC purification steps were done as described above with the exception of using Ni-Penta™ resin (Marvelgent Biosciences), Tricine-KOH buffer (pH 8.1) and 200 mM imidazole for elution. Purified PSI was stored in 25 mM Tricine-KOH (pH 8.1), 300 mM KCl, 10 % glycerol, 0.03 % β-DM. Aliquots were flash frozen and stored in liquid nitrogen.

Laser-flash spectroscopy

Samples of thylakoid membranes (60 µg Chl mL^{-1} in 5 mM HEPES-KOH, pH 7.5) or PSI particles (6 µg Chl mL^{-1} in 5 mM Tricine-KOH pH 8.0, 0.03 % β-DDM) were diluted with the same buffer containing 10 mM sodium ascorbate in the dark. A JTS-10 (Bio-Logic) kinetic spectrophotometer was used to monitor absorbance changes at 696 nm. Excitation was provided by a frequency-doubled Nd/YAG laser (532 nm) generating ~6-ns pulses (~25 mJ per pulse).

A saturating laser flash was used to create the $P_{700}^{+}(F_A/F_B)^{-}$ charge-separated state, which occurs in <1 µs.[32] Absorbance changes at 696 nm were monitored with dim 10-µs flashes before and after the laser flash (starting 250 µs after the flash) to monitor creation and decay of P_{700}^{+}. To eliminate actinic effects of the probing light and electronic artifact due to changing data collection rates, a background transient (with the laser shutter closed) was subtracted. The decay of P_{700}^{+} was fit to a sum of 2-6 exponential decay components using the Levenberg-Marquardt iteration algorithm.

Anaerobic adaptation

To allow activation of the hydrogenase enzyme, cells were harvested in early/mid-logarithmic phase (2-6 µg Chl mL^{-1}) by centrifugation (3500 *x g* for 5 min) and resuspended in fresh TAP medium at ~1-2 µg Chl mL^{-1} (for *in vivo* H_2 measurements). Ten mL of the cell suspension was placed in a 25-mL clear glass bottle sealed with stoppers, wrapped in aluminum foil and bubbled with argon (flow rate 10-15 mL min^{-1}) for 90 min in the dark, unless otherwise indicated, prior to the start of the H_2 production period. Once sparging was terminated, cells were agitated on a shaker at 160 rpm.

***In vitro* hydrogenase activity**

Cells were centrifuged and resuspended at ~30 µg Chl mL^{-1} in anaerobic adaptation buffer (50 mM potassium phosphate pH 7.2, 3 mM $MgCl_2$) and sparged with water-saturated argon for variable times in the dark in the initial experiments; the standard time was 90 min thereafter. For each reaction, 1 mL of reaction buffer (100 mM Tris-HCl, pH 7.3, 1 M NaCl, 10 mM methyl viologen, 0.2% Triton X-100) was mixed with 0.2 mL of 100 mM $Na_2S_2O_4$ (dissolved in 30 mM NaOH) in an anoxic glovebox (Coy) and sealed; the headspace of the vial was sparged with argon for 20 min to remove any residual H_2 from the glovebox gas and warmed to 37 °C prior to injection of 100 µL of cell suspension into the reaction mixture. The vial was mixed well, temperature was maintained at 37 °C with mild shaking, and aliquots of the headspace gas were removed at intervals and analyzed by gas chromatography (see below).

Gas chromatography (GC) measurements

A model SRI 310 GC equipped with a thermal conductivity detector (TCD) and molecular sieve (13X or 5A) was used for all gas measurements. A sample (80 µL) of the headspace gas was removed with a 1710RN airtight Hamilton 100-µL syringe (that had been flushed with argon) and injected into the GC. A 1% H_2/99% N_2 gas mixture (Supelco) was used to create a standard curve for H_2, and air was used as a standard for O_2 and N_2. The O_2:N_2 ratio was used to monitor for air contamination during sampling, as the headspace of all samples was primarily Ar.

Immunoblotting

Polypeptide separation and immunoblotting was performed as described previously.[20] Isolated PSI^{H6} or PSI-$HydA^{H6}$ were loaded on the basis of P_{700} photobleaching activity (see below): 1.6 pmol of P_{700} for detection of small polypeptides (PsaC, PsaD, PsaC-HydA2) or 0.4 pmol of P_{700} for detection of larger polypeptides (PsaA).

Membrane inlet mass spectrometry (MIMS) measurements

Cells grown to early log phase were spun down and resuspended to 15 µg Chl mL^{-1} in a total volume of 5 mL in TAP or TP medium (with or without acetate, respectively); 50 mM HEPES (pH 7.2) and 2 mM $NaHCO_3$ were included to maintain pH and CO_2 levels. Cell were loaded into a closed temperature-controlled (24.5° C) and stirred MIMS cuvette. Anaerobiosis was achieved in approximately 1 hour due to respiration in the dark; relevant gas masses were monitored continuously. After approximately 1 h, cells were exposed to various intensities of red light (635 nm via the actinic module of the DUAL-PAM 100 from Heinz Walz GmbH) for 2 min interspersed with 2 min darkness. Rates were calculated from the slope of the best linear fit over a 1-min period. H_2 and O_2 analysis was done by MIMS.[33] Enforced anaerobiosis with glucose oxidase and glycolaldehyde treatment were performed as described previously.[16]

Light-to-hydrogen conversion efficiency

PAR was determined with Li-COR photon counter equipped with quantum sensor (LI-190R). Efficiency calculations were performed as previously described[34] with slight modifications.

$$\eta(\%) = \frac{\left(\Delta G^{\circ} - RT\ln\frac{P^{\circ}}{P}\right)v_{H2}}{E_i A t}100$$

, where ΔG° is the standard Gibbs free energy for water oxidation (237.2 kJ mol^{-1} at 25 °C and 1 atm), *R* is the universal gas constant, *T* is absolute temperature (K), P^{o} and *P* are the hydrogen partial pressures (standard and observed, respectively), v_{H2} = amount of H_2 produced (mol), E_i = energy flux of the incident light (J m^{-2} s^{-1}), A = illuminated surface area (m^2), *t* = duration of illumination (s). Energy for the incident light was either calculated using the Planck-Einstein relation for red light at 630 nm or measured using a LI-200R pyranometer (LI-COR Biosciences, Lincoln, NE, USA) for white light.

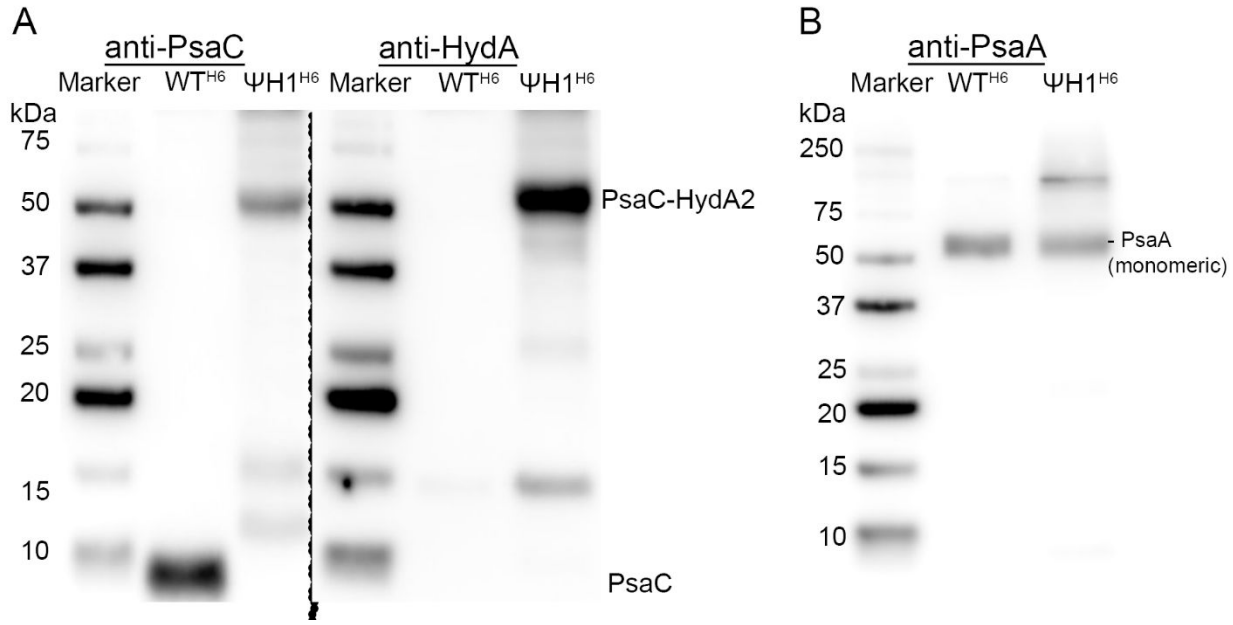

Fig. 2 Immunoblots of isolated PSI and PSI-HydA from WT^{H6} or $\Psi H1^{H6}$, demonstrating assembly of PsaC-HydA2 into PSI-HydA. Equimolar amounts of PSI and PSI-HydA were probed with α-PsaC (A, left), α-HydA (A, right), or α-PsaA (B) antibodies. Sizes of marker polypeptides are indicated to the left. Integration of α-PsaA cross-reactive bands gave a ratio of 1.00:1.09 (WT:chimera).

Results and discussion

Chimeric protein design and creation

Based on the crystal structure of cyanobacterial PSI (1JB0)[35] and a homology model of HydA2,[36] we selected the turn of a β-hairpin over the terminal F_B cluster in PsaC as the optimal insertion point for the hydrogenase domain. The entire sequence of the mature HydA2 hydrogenase from *C. reinhardtii* was inserted into this site as an in-frame fusion that would effectively split PsaC into two polypeptide segments. (See **Experimental** for details and **Fig. S1** for exact sequence of the chimeric polypeptide). The N- and C-termini of HydA2 are in close proximity,[36] in principle allowing this type of chimeric polypeptide to fold as two domains, with the HydA domain presumably folding first, allowing the two PsaC fragments to fold together. According to our modeling studies, this design would place the [4Fe-4S] cluster of HydA2 relatively close to the F_B cluster of PSI (14.8 Å edge-to-edge distance, see **Experimental** for details). The fusion gene and protein are henceforth referred to as *psaC-hydA2* and PsaC-HydA2, respectively. When co-assembled with PSI, the chimeric protein is called "PSI-HydA" (see **Fig. 1C** for a model).

The *psaC-hydA2* gene was introduced into the chloroplast genome by particle-mediated gene transfer using flanking sequences to direct homologous recombination such that it would replace the endogenous *psaC* gene.[25] Serial cloning under selective conditions was maintained until a homoplasmic state was achieved (*i.e.*, all copies of *psaC* replaced by *psaC-hydA2*), as verified by PCR (**Fig. S2**). The amplified PCR products were sequenced to ensure that no mutations in the chimeric gene had arisen during the process. The *psaC-hydA2* gene was introduced into two strains: a *hydA1-1 hydA2-1* mutant lacking endogenous hydrogenases[26] as well a strain expressing a hexahistidine-tagged (H_6) version of PsaA, a core subunit of PSI.[28] Note that in the former, PSI-HydA is the only significant contributor to hydrogen production; in both strains, WT PSI would be replaced by PSI-HydA. For brevity, the congenic D66 control strain is referred to as wild-type (WT), the *hydA1-1 hydA2-1* strain is called *hydA*, and the *hydA1-1 hydA2-1*[*psaC-hydA2*] transformant is referred to as ΨH1. The strains expressing H_6-tagged PSI are called WT^{H6} (with normal PsaC) or $\Psi H1^{H6}$ (with PsaC-HydA2).

Subunit composition of PSI-HydA chimera

PSI and PSI-HydA were purified from WT^{H6} and $\Psi H1^{H6}$, respectively, via immobilized metal affinity chromatography.[28] Purified complexes were denatured with SDS and equivalent amounts of PSI were analyzed by immunoblotting with antibodies against PSI subunits and hydrogenase, to assess the subunit composition of the complexes. The anti-PsaC antibody recognized a ~9-kDa polypeptide in WT PSI (**Fig. 2A, left**), consistent with its predicted size (8.8 kDa). This polypeptide was not observed in the PSI-HydA complex; instead, a new ~52-kDa polypeptide was seen, similar to the predicted size of the PsaC-HydA2 polypeptide (56 kDa). Probing with anti-HydA antibodies revealed a polypeptide of the same size in PSI-HydA complexes, but not in WT PSI (**Fig. 2A, right**). Thus, PSI complexes in this strain incorporate PsaC-HydA2 rather than PsaC.

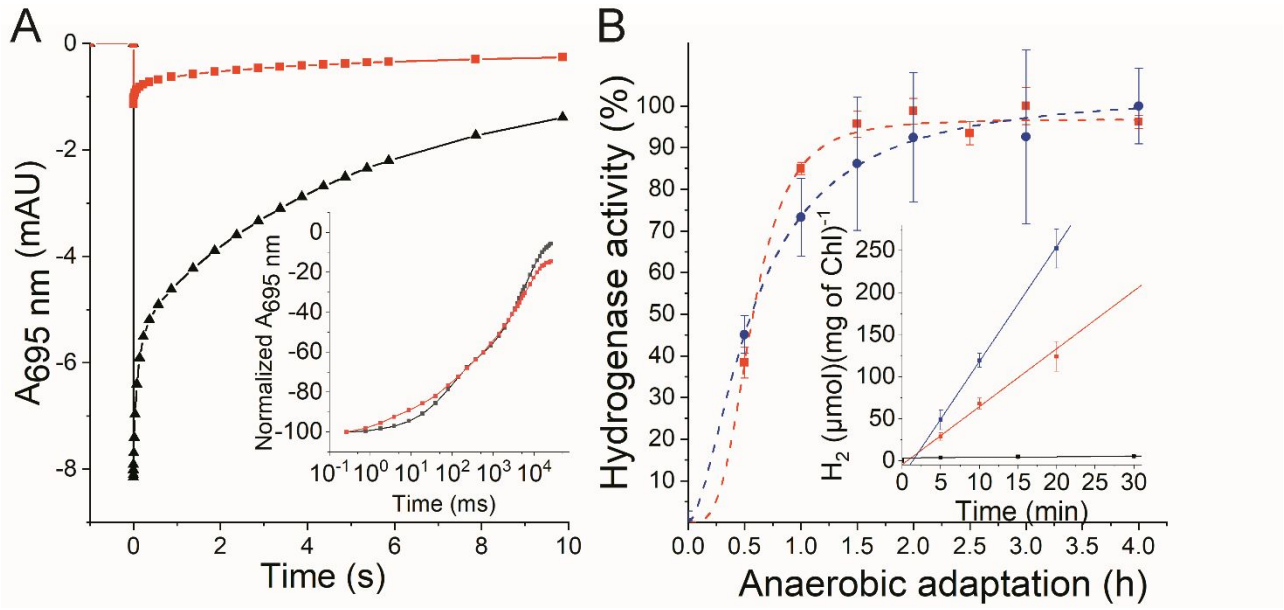

Fig. 3 *In vitro* characterization of the PSI-hydrogenase chimera. **(A)** Transients of flash-induced P_{700} photobleaching and recovery in thylakoid membranes (60 µg Chl) isolated from *hydA* (black) and ΨH1 (red) cells that had been grown aerobically. The inset displays transients normalized to the maximal bleaching and using a log time scale. **(B)** Hydrogenase activity (expressed as % of maximal activity attained) assayed with reduced MV on whole cells, as a function of the anaerobic adaptation period. Inset: In vitro H_2 production with dithionite/MV in detergent-permeabilized *hydA* (black), WT (blue), and ΨH1 (red) cells after 1.5 h anaerobic induction. Error bars represent standard error (n=3).

Roughly equal amounts of PsaA were detected in PSI and PSI-HydA (1.0:1.1; **Fig. 2B**) when the lanes were loaded on the basis of equal photochemical activity (see **Fig. 3A**), implying that >90% of the PSI-HydA in the ΨH1 cells is photochemically active. We would not expect any unassembled PsaA polypeptide to be present, as it has been shown that the quality control system of the chloroplast keeps the level of unassembled subunits of PSI or other multi-subunit complexes very low.[37]

Based on the structure of cyanobacterial PSI,[35] as well as mutagenesis[38] and modeling[39] studies, it is thought that the Fd-docking site of PSI is formed by PsaC in concert with PsaD. The structure of PSI reveals an intimate interaction between PsaC and a long C-terminal extension of PsaD, and the addition of the HydA domain in the fusion had the potential to interrupt this interaction and prohibit assembly of PsaD into the complex. However, we found that the level of PsaD in the purified PSI complexes was similar in both preparations (**Fig. S3**), consistent with our model of PSI-HydA (**Fig. 1C**).

Activities of the PSI-HydA chimera *in vitro*

Laser-flash spectroscopy experiments were performed to assess the photochemical activity of the PSI portion of the PSI-HydA chimera. P_{700} is a pair of Chl *a* molecules serving as the primary electron donor in PSI. Excitation of PSI produces a charge-separated state in which P_{700} is oxidized (P_{700}^+) and the terminal acceptor is reduced. In the absence of an electron acceptor, the rate of charge recombination is characteristic of the charge-separated state; for example, charge recombination of $P_{700}^+(F_A/F_B)^-$ occurs in 40-200 ms, but is >50 times faster from the prior charge-separated state ($P_{700}^+F_X^-$).[18] In the absence of the PsaC subunit, the PsaA/PsaB heterodimer is degraded and does not accumulate in *C. reinhardtii*.[40] Therefore, the level of photoactive PSI can be used to assess the ability of PsaC-HydA2 to assemble with and stabilize the PSI core. The amount of photo-bleachable P_{700} in thylakoid membranes isolated from ΨH1 was ~15% that of WT (**Fig. 3A**). The lowered accumulation of PSI-HydA was not unexpected, given that point mutations of single residues in PSI can result in more drastic effects.[25] The kinetics of fast P_{700}^+ decay (**Fig. 3A inset**) are very similar in PSI and PSI-HydA, indicating that the F_A and F_B clusters must be properly assembled within the PsaC domain of the chimeric protein (**Table S1, Supplementary text**). Oxygen can readily accept electrons from PSI effectively quenching back reactions with longer lifetimes and contributing to overall "electron escape" that must be replenished by an exogenous electron donor (*i.e.*, ascorbate). In order to get a better understanding of charge recombination kinetics in the PSI-HydA2 chimera, we prepared PSI complexes anoxically from anaerobically adapted WT^{H6} and $ΨH1^{H6}$ cultures. As seen in **Fig. S4A**, electron escape is reduced in both preparations to ~24% (**Fig. S4B**), and there is the typical biphasic kinetics of charge recombination from the $P_{700}^+(F_A/F_B)^-$ state in the 40-200 ms time range. In the PSI-HydA2 chimera, there are 3 new kinetic phases. The fastest two represent charge recombination of the $P_{700}^+F_X^-$ state, and together represent ~12% of the total decay, indicating that the association of PsaC-HydA2 with PSI may be weaker than PsaC and some of it dissociates during purification. There is also a new component with a lifetime of 550-600 ms, representing ~9% of the total decay. We tentatively assign this to charge recombination from the [4Fe-4S] cluster of the HydA2 domain.

The HydEF/G maturases are required for insertion of the di-iron site into the HydA domain after assembly of the [4Fe-4S] cluster by the chloroplast SUF machinery[41], and it was unclear if the maturases would be able to access the HydA domain in the new chimeric context. The hydrogenase activity of cells expressing PSI-HydA was assessed in detergent-permeabilized cells with

reduced methyl viologen (MV) as electron donor. We found that maximal hydrogenase activity was attained within 1.5 hours after a shift to anaerobiosis, similar to what was shown for WT hydrogenases in *C. reinhardtii.* [15] (**Fig. 3B**). The parental *hydA* strain exhibited a very slow rate of H_2 production (~4.1 ± 0.2 µmol h^{-1} (mg Chl)$^{-1}$), as expected, while the WT rate was 770 ± 50 µmol h^{-1} (mg Chl)$^{-1}$). The H_2 production rate in permeabilized ΨH1 cells was linear with time over the 20-min time course, similar to the permeabilized WT cells, indicating that the hydrogenase domain in PSI-HydA was not unstable (**Fig. 3B inset**). They produced H_2 at a rate of ~380 ± 80 µmol h^{-1} (mg Chl)$^{-1}$. Since the hydrogenase activity in the parental strain is ~1% of this, nearly all of the H_2 produced by the ΨH1 cells can be attributed to the PSI-HydA chimera. Using the extinction coefficient of P_{700},[42] we estimate the amount of PSI-HydA in the ΨH1 strain as 1 per 5650 Chl. If each PSI-HydA had an active hydrogenase, the turnover frequency for PSI-HydA would be ~530 ± 110 H_2 s^{-1}. This number is comparable with the reported specific activity of HydA1 using a similar assay (380 ± 97 µmol H_2 min^{-1} mg^{-1}),[10] which is equivalent to a turnover frequency of ~300 H_2 s^{-1}. Thus, it seems likely that all of the HydA domains in the PSI-HydA chimeric complexes are fully active after the anaerobic induction period.

Addition of the large HydA domain to PsaC was expected to block its access to electron acceptors such as Fd. This was tested *in vitro* by assaying the purified protein for light-dependent reduction of low-potential electron acceptors in the presence of ascorbate, a high-potential electron donor. The PSI-HydA chimera exhibited a ~9-fold drop in light-driven reduction of cyanobacterial flavodoxin (**Fig. S5A**). This protein replaces Fd in cyanobacteria grown in low iron, and has been shown to bind to both cyanobacterial and algal PSI in the same mode as Fd.[43] In contrast, the ability of PSI-HydA to reduce algal Fd (in a coupled assay) was reduced by only 50% (**Fig. S5B**). Photoreduction of O_2 to superoxide (*i.e.*, Mehler reaction) was ~2-fold *higher* in PSI-HydA (**Fig. S5C**), proving that overall electron flow was not compromised by addition of the HydA domain. These assays were performed in air, where the di-iron site would be inactivated (*i.e.*, no competition with proton reduction), but the [4Fe-4S] cluster should still be present in the HydA domain.[4] Both algal Fd and cyanobacterial flavodoxin bind the same site on PsaC involving Lys35,[44,45] which is absent in PSI-HydA; thus, one would expect both proteins to have lost their high-affinity binding site on PSI. An explanation for the difference between their behavior with PSI-HydA is that it is the HydA domain that reduces them, rather than PsaC. The algal hydrogenase is reversible; the HydA domain binds Fd, oxidizing it when producing H_2, and reducing it when oxidizing H_2.[16] Access to the Fd-binding site of HydA2 is not expected to be blocked in the PSI-HydA chimera. Thus, Fd reduction by PSI-HydA likely proceeds via the HydA [4Fe-4S] cluster to Fd bound to its interaction site on HydA. The algal HydA domain would not be expected to bind the cyanobacterial flavodoxin very well, explaining the much lower photoreduction rate with this electron acceptor. The higher O_2 photoreduction rate of PSI-HydA may reflect a higher rate of O_2 reduction from the HydA [4Fe-4S] cluster than from the F_A/F_B clusters of PsaC.

Production of H_2 and O_2 *in vivo*

The ability of the hydrogenase domain in PSI-HydA to carry out H_2 production during dark fermentative conditions, in which Fd is largely reduced by pyruvate:Fd oxidoreductase,[46] was assessed by gas chromatography using a thermal conductivity detector (GC-TCD). Slow accumulation of H_2 in the headspace was observed in the cultures incubated in the dark (**Fig. 4A**). Hydrogen did not accumulate to detectable levels in the *hydA* culture until after 6 h and the rate was extremely low thereafter (8 ± 5 nmol H_2 h^{-1} (mg Chl)$^{-1}$). The rate of H_2 production by ΨH1 was roughly 60% of the WT rate [330 ± 10 nmol H_2 h^{-1} (mg Chl)$^{-1}$ vs 507 ± 30 nmol H_2 h^{-1} (mg Chl)$^{-1}$] and remained fairly constant throughout the 6-hour experiment (see **Fig. 4A**). This ratio of activities is similar to the ratio of maximal H_2 production rate measured in these cells (**Fig. 3B**), indicating that the HydA2 domain in the PSI-HydA chimera is fully able to accept electrons via its normal physiological donor (Fd), consistent with the conclusion above that the HydA2 domain of the PSI-HydA chimera can bind and reduce Fd.

Illumination of the anoxic WT culture resulted in transient H_2 production, as observed previously.[16,47] The average rate was 28 ± 8 µmol H_2 h^{-1} (mg Chl)$^{-1}$ during the first hour, but rapidly dropped to negligible levels thereafter (**Fig. 4B**). The *hydA* strain did not make any detectable H_2. In contrast, ΨH1 produced H_2 continuously for 6 h, with an initial rate of ~25 ± 6 µmol H_2 h^{-1} (mg Chl)$^{-1}$ in the first hour and an average rate of 21 ± 6 µmol H_2 h^{-1} (mg Chl)$^{-1}$ over the entire time course.

Like many redox enzymes catalyzing low-potential redox reactions, the algal hydrogenase is inactivated by O_2. One of the reasons for sustained H_2 production by ΨH1 is that O_2 does not accumulate in the sealed culture, unlike WT or *hydA* (**Fig. S6**). To test the hypothesis that the ΨH1 strain consumes O_2 faster than it is produced, we measured net O_2 rise/fall in aerobic cultures. The compensation point is the light intensity at which O_2 production by PSII is matched by O_2 consumption. Even up to the brightest light used, the ΨH1 culture with acetate never reached this point, while the culture lacking acetate required a light intensity ~5 times that of the parental strain to reach compensation. Acetate decreases net O_2 evolution via its effects on photosynthesis and mitochondrial respiration.[48] Light-dependent net O_2 evolution rates were ~35% lower in ΨH1 compared to the parental strain (**Fig. S7**). This could stem from either higher respiration rates or lower photosynthesis rates. In fact, we did not observe higher dark respiration rates in ΨH1 (**Fig. S7A**). Lower rates of water oxidation could be due to either lower PSII activity or to limitations in electron flow downstream of PSII. We found that addition of phenyl-1,4-benzoquinone (PPBQ) as an artificial PSII electron acceptor resulted in similar light-dependent O_2 evolution rates in the two strains (**Fig. S7B**), consistent with the latter hypothesis. Additionally, the quantum yield of PSII drops to low values at fairly low light intensities in the light saturation curve (**Fig. S7C**), consistent with a highly reduced plastoquinone pool and a limitation in downstream electron flow. This is almost certainly due to the PSI-HydA chimera, whose abundance is ~7-fold lower than WT PSI. Thus, it appears that the bottleneck induced by lowered accumulation of the chimeric protein had the effect of constraining PSII O_2

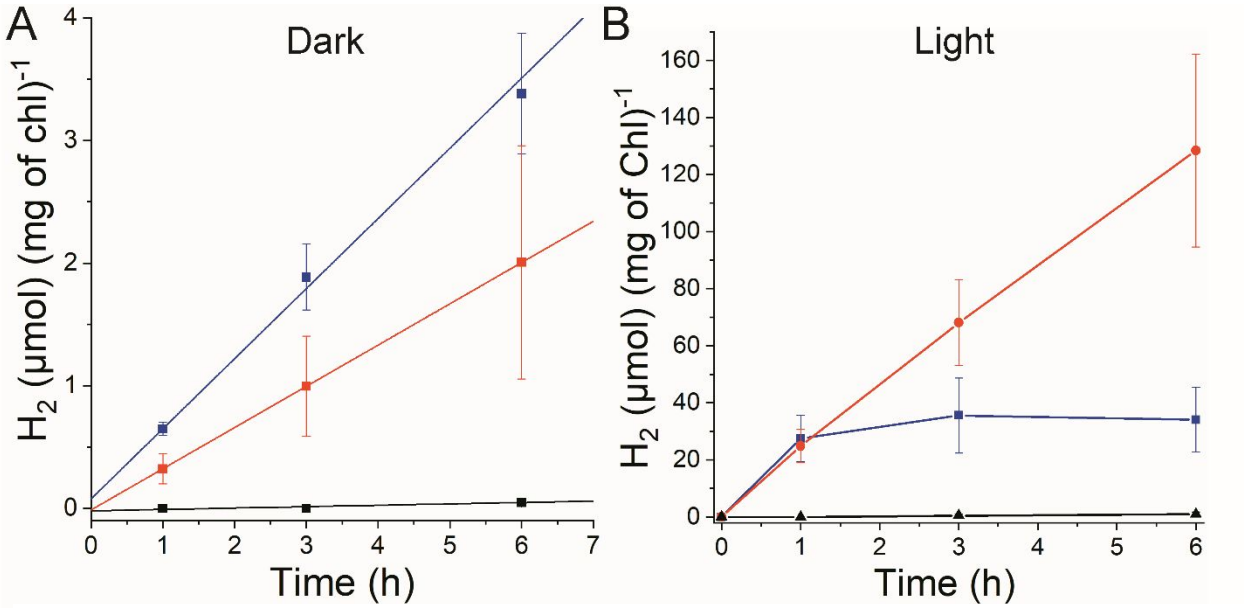

Fig.4 Accumulated H_2 in the headspace of sealed bottles produced by WT (blue), *hydA* (black), or ΨH1 (red) cultures in dark (A) or light (B, 200 µmol photons m^{-2} s^{-1}), as measured by GC-TCD (n=3). Values are normalized to the initial Chl content of the cultures. Please note the different scales.

evolution activity such that respiration and other O_2-consuming processes could keep up with it. While this was an *unintended* consequence of the PSI-HydA design, it resulted in preserving hydrogenase activity for sustained H_2 production. However, as many other redox enzymes are sensitive to O_2 and lowered abundance of chimeric proteins is a likely occurrence, this actually bodes well for the approach of fusing such enzymes to PSI.

To quantify the instantaneous rates of H_2 and O_2 production by the algal cells, an online membrane inlet mass spectrometry (MIMS) technique was used to measure dissolved gasses during short illumination times (<2 min). The ΨH1 cells exhibited a significantly higher H_2 evolution than WT at photon fluxes above ~300 µmol m^{-2} s^{-1} and did not saturate until over ~1000 µmol photons m^{-2} s^{-1} (**Fig. 5A**). In stark contrast, H_2 production by WT cells saturated at lower light intensities (~100 µmol photons m^{-2} s^{-1}) with a maximum rate of 11 ± 4 µmol H_2 h^{-1} (mg Chl)$^{-1}$, regardless of the presence of acetate. There was no detectable H_2 production by *hydA* cells. For ΨH1 cells, the highest observed rates were 76 ± 11 or 49 ± 6 µmol H_2 h^{-1} (mg Chl)$^{-1}$ in media with or without acetate, respectively. To eliminate the effect of O_2 inhibition on hydrogenase activity, we added glucose, glucose oxidase, and catalase to the medium to scavenge O_2.[16] With saturating light, the highest observed rate was 90 ± 5 µmol H_2 h^{-1} (mg Chl)$^{-1}$, representing a ~20% improvement (**Fig. 5C**). Fitting of the data to a hyperbolic curve allowed us to estimate V_{max} to be 120 µmol H_2 h^{-1} (mg Chl)$^{-1}$ with half-saturation at 340 µmol photons m^{-2} s^{-1}. (In order to compare this maximal rate to those of chemotrophs or abiotic materials, it is equivalent to 2.7 mmol H_2 h^{-1} per g dry weight of cells.) To put this in context, such a strain could perform well even on a cloudy day (~600 µmol m^{-2} s^{-1}) and still reach saturation on a sunny day (≥2000 µmol m^{-2} s^{-1}).[49] Although the algal [FeFe] hydrogenase is known to be irreversibly inhibited by O_2 in a matter of seconds[50] and PSII is producing O_2 in the same membrane, O_2 scavenging only improved H_2 production in the ΨH1 culture by 20%. This demonstrates that keeping the enzyme in its cellular context allows maintenance of its activity for much longer periods than might be expected.

We now turn to the possible sinks in ΨH1 cells for electrons from PSII. A major motivation for our design was to intercept electrons from the PETC before they reached the Fd pool. Examination of **Figure 5** allows one to conclude that the majority of these electrons are used to make H_2 in the ΨH1 strain. In the absence of acetate, maximal net O_2 production in the WT culture is ~45 µmol O_2 h^{-1} (mg Chl)$^{-1}$. Although we do not know the respiration rate in these short-term experiments, it cannot be high, as the cultures start out anoxic before illumination. Moreover, we know that PSII is much more constrained in ΨH1 cells than in WT cells. Therefore, we would not expect the rate of gross O_2 production by PSII in the ΨH1 culture to be higher than ~50 µmol O_2 h^{-1} (mg Chl)$^{-1}$, leading to an estimated maximal H_2 production rate ≤100 µmol O_2 h^{-1} (mg Chl)$^{-1}$, if all electrons from water oxidation were used to produce H_2. In the presence of acetate, maximal net H_2 production in the ΨH1 culture was ~75 µmol H_2 h^{-1} (mg Chl)$^{-1}$. To test this hypothesis further, we assessed the impact of competition with CO_2 fixation by using a phosphoribulokinase inhibitor (glycolaldehyde) to block the CBB cycle.[51] In the WT culture, the H_2 evolution rate quickly dropped after ~1 minute, decreasing over 10-fold from the peak rate within 5 minutes (**Fig. 5D**). This drop was largely due to the activation of the CBB cycle, as addition of glycolaldehyde resulted in a much lower drop (~50%) in H_2 evolution, which persisted during the experiment (10 min), as previously reported.[16] In contrast, the ΨH1 culture exhibited very stable H_2 production rates over the time course, and a ~20% *decrease* in H_2 evolution rate was seen after addition of glycolaldehyde. Nevertheless, we found that the ΨH1 strain was able to grow photoautotrophically, albeit much more slowly than strains containing WT PSI, and only if the culture was first rendered anoxic (**Fig. S9**). These results are consistent with the hypothesis that PSI-HydA reduces Fd *in vivo*

poorly, and directs *most*, but not all, of the electrons from the PETC to proton reduction, at least under high light (discussed further below). We also found that cyclic electron flow around PSI was negligible in ΨH1 cells (**Fig. S10**), consistent with this idea. Thus, both linear and cyclic electron transport pathways are strongly affected in ΨH1 cells, demonstrating that photosynthetic electron flow has effectively been redirected in these cells by replacement of PSI with PSI-HydA. When one considers that the amount of PSI is ~7-fold lower (**Fig. 3A**) and the total amount of hydrogenase activity is ~2-fold lower (**Fig. 3B**) in the ΨH1 strain compared to WT, and yet the instantaneous light-saturated H_2 production rate is almost 7-fold higher than WT in this strain, it is difficult to imagine how this could be, unless electrons from PSI were being directly delivered to the hydrogenase active site, as intended by the chimeric protein design.

We tested the utility of this system for long-term H_2 production. After anoxia was imposed in a sealed bottle, the culture produced H_2 continuously for 5 days at an average rate of 14.0 ± 1.7 µmol H_2 h^{-1} (mg Chl)$^{-1}$ (**Fig. S8A**). A similar experiment was run without imposing anoxia, and within 2 days the ΨH1 culture had become hypoxic (~4% O_2 in the headspace) and started producing H_2 (**Fig. S8B**). We also set up long-term experiments using a PBR in turbidostat mode, which was flushed continuously with argon. Hydrogen was monitored in the efflux gas, allowing calculation of the rate of H_2 production by the culture. Cultures were maintained at high density (~ 30 mg Chl L^{-1}) under continuous illumination (600 µmol photons m^{-2} s^{-1}). The production rate was 86.6 ± 2.4 mL H_2 d^{-1} per L culture (n=3). These rates, whether in sealed bottles or in a PBR, are at least comparable to rates reported in this species using the endogenous hydrogenases in concert with other methods to

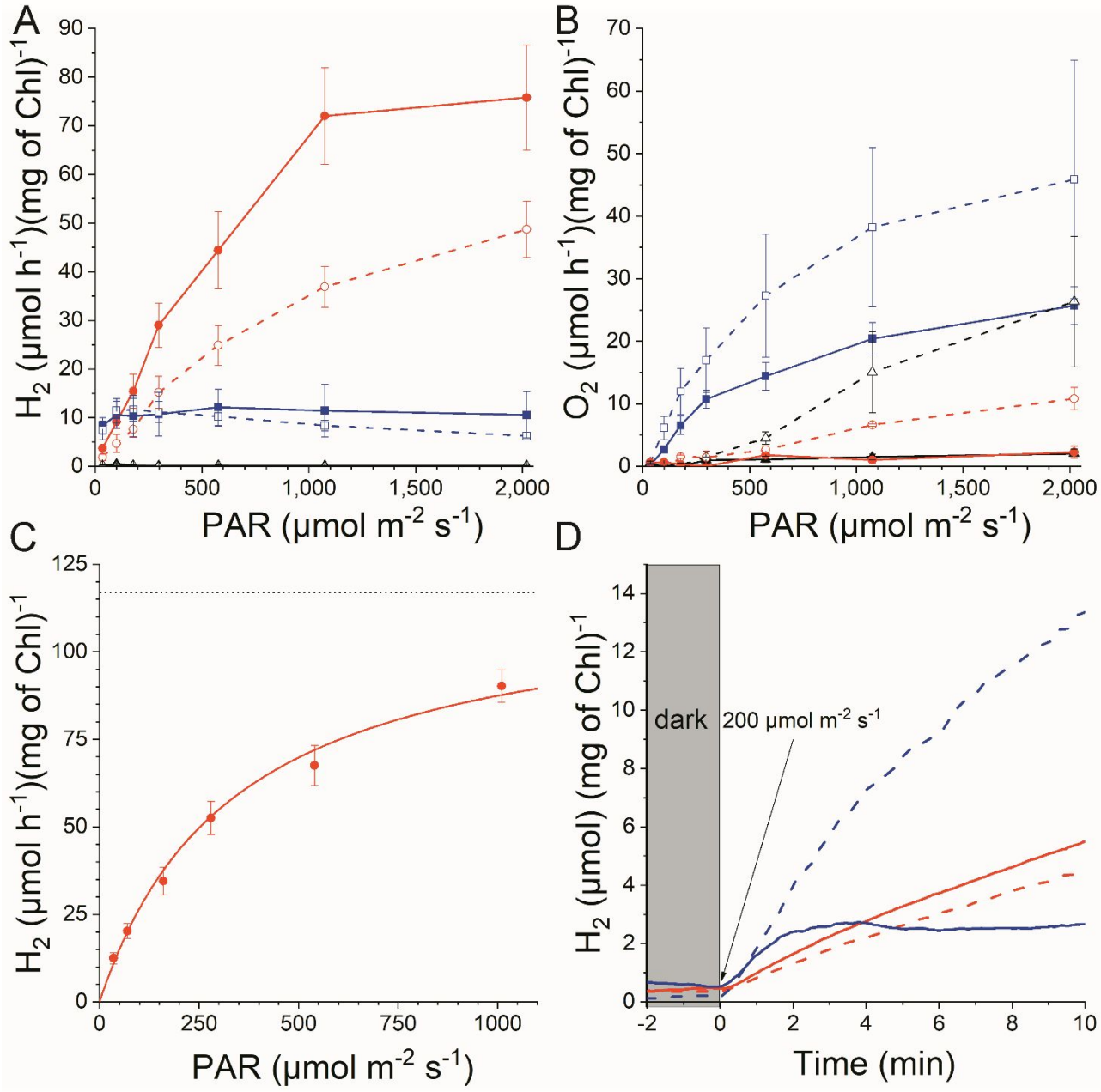

Fig. 5. Membrane inlet mass spectrometry (MIMS) data. Rates of H_2 **(A)** or O_2 **(B)** production in cultures of WT (blue), *hydA* (black), and ΨH1 (red) under indicated light intensities in media containing acetate (solid symbols/lines) or lacking acetate (hollow symbols/dashed lines). Rates were determined as the slope of concentration change over 1 min of time. **(C)** Effect of enforced anoxia using glucose oxidase/catalase on H_2 evolution rate in an anaerobically adapted ΨH1 culture with acetate. Light-saturation data were fitted to a hyperbolic curve with V_{max} (dotted line) ~120 µmol of H_2 h^{-1} (mg of Chl)$^{-1}$. Error bars in A-C represent standard error of the mean (biological replicates, n=3). **(D)** Instantaneous H_2 production normalized to Chl under enforced anoxia of ΨH1 (red) or WT (blue) cultures with (dashed lines) or without (solid lines) 60 mM glycolaldehyde under continuous 200 µmol m^{-2} s^{-1} red light (average of 3 biological replicates).

lower steady-state O_2 levels and/or direct electrons to H_2 production.[8] In order to compare this rate to H_2 production rates using chemotrophs or abiotic materials, we normalized to dry weight of cells rather than Chl to obtain a rate of 164 ± 5 mL H_2 d^{-1} g^{-1}. The light-to-hydrogen conversion efficiency of ΨHI cultures reached 1.75% under the best conditions (*i.e.*, short term with acetate and enforced anoxia, using 6.65 W m^{-2} of 630-nm photons), which is just over 10% of the theoretical maximum. While this is encouraging, we are still far from realizing the full potential of the system on a long-term basis, as light-to-hydrogen conversion efficiency was only about 0.12% in the aforementioned PBR experiment.

It is somewhat surprising that marrying two very different proteins resulted in such an active chimeric protein. Using the maximal rate estimated from the MIMS experiment, and taking into account the PSI-HydA cellular abundance, one arrives at a H_2 production rate of ~170 H_2 s^{-1} for each PSI-HydA (*i.e.*, ~340 electrons s^{-1}). This is in line with previously reported electron throughput rates for PSI.[52] It also compares favorably with the PSI-hydrogenase assembly created *in vitro* that is currently the best *in vitro* H_2 photoproduction device (~50 H_2 s^{-1}).[53] In both cases, the overall throughput is likely limited by electron donation to P_{700}. The PSI-HydA chimera may have an advantage there, as algal Pc can reduce P_{700} in <50 µs.[54] Based on these calculations, we conclude that the PSI-HydA chimera reported here is actually a very efficient light-driven proton photoreduction machine, capable of producing a dihydrogen every ~6 ms *in vivo*.

It is important to realize that the addition of the hydrogenase domain to PSI has created a photosystem that is fundamentally different from PSI, which is a type I reaction center that oxidizes and reduces 1-electron carriers. The PSI-HydA chimera requires 2 electrons to produce 1 H_2. Thus, it first needs to accumulate one electron on the HydA domain; after re-reduction of P_{700}^+ by plastocyanin and excitation of the reaction center, a second electron can be sent to the hydrogenase active site (see **Fig. 1C**), resulting in reduction of 2 protons to a dihydrogen molecule. This is more akin to the action of a type II photochemical reaction center, which accumulates 2 electrons to reduce a quinone to quinol (also consuming 2 protons), although in this case the product is a *gaseous* molecule. Thus, it is not an overstatement to say that we have created a novel photochemical reaction center by fusing hydrogenase to PSI. It is also important to consider the competition between reduction of Fd (requiring 1 electron) and protons (requiring 2 electrons). The longer the delay between the first and second electron arriving at the H-cluster, the more time that Fd has to bind to the HydA domain and "steal" the electron. This almost certainly explains the very high light flux required to saturate H_2 production in the ΨH1 cultures (**Fig. 5A**), as higher light intensities will result in shorter average delays between consecutive excitations of PSI-HydA. Thus, as such a culture went through a day-night cycle, it would be biased towards Fd reduction at the beginning and end of the day, allowing it to fulfill basic physiological needs, but be biased towards H_2 production in the middle of the day, storing some of the energy of the extra photons as molecular hydrogen.

Future efforts to increase H_2 production with this system will focus on use of more O_2-tolerant hydrogenases. This would in turn allow use of PSI-HydA chimeras that accumulated to higher levels. While that would increase H_2 production, it would allow more O_2 production. However, as long as the steady-state level of O_2 present in the flow PBR system were not higher than the tolerance of the hydrogenase domain, the system should be able to produce H_2 continuously at a rate significantly higher than reported here. It should also be possible to modulate the partitioning of electrons between reduction of Fd and protons by modifying the Fd binding site of the HydA domain.

Conclusions

Use of the PSI-HydA chimera offers at least 4 advantages: (1) it constitutively expresses the chimeric protein; (2) it directs the majority of electrons from water oxidation to H_2 production; (3) it constrains O_2 evolution from PSII, preserving hydrogenase activity for sustained H_2 production over many days, obviating the need to use nutrient deprivation, PSII inhibitors or mutations; and (4) it preserves the proton pumping and ATP production carried out by the PETC, thus maintaining cell viability. By rewiring photosynthesis to deliver electrons from PSI directly to hydrogenase – thus cutting out the Fd 'middleman' – one is no longer at the mercy of cellular metabolic networks. With the system entirely encoded by the algal chloroplast genome, the use of directed evolution techniques to improve the system also becomes possible. Perhaps more important than this particular example, however, is the discovery of a site in PSI that allows in-frame fusion of a protein to intercept electrons from PSI. The F_A/F_B clusters of PSI are at a lower reduction potential than any soluble electron carrier in the cell (*e.g.*, Fd, NADPH, thioredoxin). This opens the ability to drive novel redox chemistries not native to plants and algae at high flux by using a large fraction of the electrons from water-splitting and the PETC.

Conflicts of interest

There are no conflicts to declare.

Acknowledgements

We thank Dr. Gregory Orf and Prof. Derek Cashman for helpful discussions regarding homology modeling, Zachary Dobson and Christine Lewis of Prof. Petra Fromme's lab for assistance with the O_2 electrode measurements, Prof. Anne Jones and her current and former lab members, especially Dr. Joseph Laureanti and Dr. Christina Forbes, for their assistance with initial GC measurements and the use of their instrument, as well as undergraduate researchers Imran Hussain, Alec Smith and Taryn O'Boyle.

Funding: This material is based upon work supported by the National Science Foundation under Grant No. CBET-1706960. The Tel Aviv University group was supported by the Israel Science Foundation award 1646/16, the NSF-BSF Energy for Sustainability grant 2016666, and Israel Science Foundation award 2185/17.

Notes and references

† Values were derived using these parameters: k_{cat}(HydA1)= 450 s^{-1} [14]; k_{cat}(FNR)= 90 s^{-1} [12]; Fd concentration in spinach chloroplast is 4.4 nmol/(µmol of Chl)[55]; each TAP-grown *C. reinhardtii* cell contains 1 chloroplast with a volume of 130 μm^3 [56] and 3.5 fmol Chl [57].

1 S. S. Veeravalli, S. R. Shanmugam, S. Ray, J. A. Lalman and N. Biswas, in *Advanced Bioprocessing for Alternative Fuels, Biobased Chemicals, and Bioproducts*, ed. M. B. T.-A. B. for A. F. Hosseini Biobased Chemicals, and Bioproducts, Elsevier, 2019, pp. 289–312.

2 K. D. Swanson, M. W. Ratzloff, D. W. Mulder, J. H. Artz, S. Ghose, A. Hoffman, S. White, O. A. Zadvornyy, J. B. Broderick, B. Bothner, P. W. King and J. W. Peters, *J. Am. Chem. Soc.*, 2015, **137**, 1809–1816.

3 N. Nelson and A. Ben-Shem, *Nat. Rev. Mol. Cell Biol.*, 2004, **5**, 971.

4 D. W. Mulder, E. S. Boyd, R. Sarma, R. K. Lange, J. A. Endrizzi, J. B. Broderick and J. W. Peters, *Nature*, 2010, **465**, 248–251.

5 M. C. Posewitz, P. W. King, S. L. Smolinski, L. Zhang, M. Seibert and M. L. Ghirardi, *J. Biol. Chem.*, 2004, **279**, 25711–25720.

6 B. Ghysels, D. Godaux, R. F. Matagne, P. Cardol and F. Franck, *PLoS One*, , DOI:10.1371/journal.pone.0064161.

7 G. Torzillo, A. Scoma, C. Faraloni and L. Giannelli, *Crit. Rev. Biotechnol.*, 2015, **35**, 485–496.

8 S. Z. Tóth and I. Yacoby, *Trends Biotechnol.*, 2019, **37**, 1159–1163.

9 I. Yacoby, S. Pochekailov, H. Toporik, M. L. Ghirardi, P. W. King and S. Zhang, *Proc. Natl. Acad. Sci.*, 2011, **108**, 9396–9401.

10 D. Nikolova, C. Heilmann, S. Hawat, P. Gäbelein and M. Hippler, *Photosynth. Res.*, 2018, **137**, 281–293.

11 P. Decottignies, P. Lemarechal, J. P. Jacquot, J. M. Schmitter and P. Gadal, *Arch. Biochem. Biophys.*, 1995, **316**, 249–259.

12 P. Decottignies, V. Flesch, C. Gérard-Hirne and P. Le Maréchal, *Plant Physiol. Biochem.*, 2003, **41**, 637–642.

13 M. Winkler, S. Kuhlgert, M. Hippler and T. Happe, *J. Biol. Chem.*, 2009, **284**, 36620–36627.

14 G. VONABENDROTH, S. STRIPP, A. SILAKOV, C. CROUX, P. SOUCAILLE, L. GIRBAL and T. HAPPE, *Int. J. Hydrogen Energy*, 2008, **33**, 6076–6081.

15 T. HAPPE and J. D. NABER, *Eur. J. Biochem.*, 1993, **214**, 475–481.

16 Y. Milrad, S. Schweitzer, Y. Feldman and I. Yacoby, *Plant Physiol.*, 2018, **177**, 918–926.

17 S. Kosourov, M. Jokel, E. M. Aro and Y. Allahverdiyeva, *Energy Environ. Sci.*, 2018, 1–2.

18 K. Brettel, *Biochim. Biophys. Acta - Bioenerg.*, 1997, **1318**, 322–373.

19 M. Forestier, P. King, L. Zhang, M. Posewitz, S. Schwarzer, T. Happe, M. L. Ghirardi and M. Seibert, *Eur. J. Biochem.*, 2003, **270**, 2750–2758.

20 K. Reifschneider-Wegner, A. Kanygin and K. E. Redding, *Int. J. Hydrogen Energy*, 2014, **39**, 3657–3665.

21 A. Sawyer, Y. Bai, Y. Lu, A. Hemschemeier and T. Happe, *Plant J.*, 2017, **90**, 1134–1143.

22 L. A. Kelley, S. Mezulis, C. M. Yates, M. N. Wass and M. J. E. Sternberg, *Nat. Protoc.*, 2015, **10**, 845–858.

23 D. Kozakov, D. R. Hall, B. Xia, K. A. Porter, D. Padhorny, C. Yueh, D. Beglov and S. Vajda, *Nat. Protoc.*, 2017, **12**, 255.

24 A. Fiser, R. K. G. Do and A. Šali, *Protein Sci.*, 2000, **9**, 1753–1773.

25 N. Fischer, P. Sétif and J. D. Rochaix, *Biochemistry*, 1997, **36**, 93–102.

26 J. E. Meuser, S. D'Adamo, R. E. Jinkerson, F. Mus, W. Yang, M. L. Ghirardi, M. Seibert, A. R. Grossman and M. C. Posewitz, *Biochem. Biophys. Res. Commun.*, 2012, **417**, 704–709.

27 N. Fischer, O. Stampacchia, K. Redding and J.-D. Rochaix, *Mol. Gen. Genet. MGG*, 1996, **251**, 373–380.

28 G. Gulis, K. V Narasimhulu, L. N. Fox and K. E. Redding, *Photosynth. Res.*, 2008, **96**, 51–60.

29 Y. Li, M.-G. Lucas, T. Konovalova, B. Abbott, F. MacMillan, A. Petrenko, V. Sivakumar, R. Wang, G. Hastings, F. Gu, J. van Tol, L.-C. Brunel, R. Timkovich, F. Rappaport and K. Redding, *Biochemistry*, 2004, **43**, 12634–12647.

30 J. Kropat, A. Hong-Hermesdorf, D. Casero, P. Ent, M. Castruita, M. Pellegrini, S. S. Merchant and D. Malasarn, *Plant J.*, 2011, **66**, 770–780.

31 R. J. Porra, W. A. Thompson and P. E. Kriedemann, *Biochim. Biophys. Acta - Bioenerg.*, 1989, **975**, 384–394.

32 M. Byrdin, S. Santabarbara, F. Gu, W. V Fairclough, P. Heathcote, K. Redding and F. Rappaport, *Biochim. Biophys. Acta - Bioenerg.*, 2006, **1757**, 1529–1538.

33 O. Liran, R. Semyatich, Y. Milrad, H. Eilenberg, I. Weiner and I. Yacoby, *Plant Physiol.*, 2016, **172**, 264–271.

34 S. Kosourov, M. Jokel, E. M. Aro and Y. Allahverdiyeva, *Energy Environ. Sci.*, 2018, **11**, 1431–1436.

35 P. Jordan, P. Fromme, H. T. Witt, O. Klukas and others, *Nature*, 2001, **411**, 909.

36 C. H. Chang, P. W. King, M. L. Ghirardi and K. Kim, *Biophys. J.*, 2007, **93**, 3034–3045.

37 O. Ostersetzer and Z. Adam, *Plant Cell*, 1997, **9**, 957–965.

38 P. Sétif, N. Fischer, B. Lagoutte, H. Bottin and J. D. Rochaix, *Biochim. Biophys. Acta - Bioenerg.*, 2002, **1555**, 204–209.

39 D. J. Cashman, T. Zhu, R. F. Simmerman, C. Scott, B. D. Bruce and J. Baudry, *J. Mol. Recognit.*, 2014, **27**, 597–608.

40 Y. Takahashi, M. Goldschmidt-Clermont, S. Y. Soen, L. G. Franzén, J. D. Rochaix, L. G. Franzen and J. D. Rochaix, *EMBO J.*, 1991, **10**, 2033.

41 E. M. Shepard, F. Mus, J. N. Betz, A. S. Byer, B. R. Duffus, J. W. Peters and J. B. Broderick, *Biochemistry*, 2014, **53**, 4090–4104.

42 H. Witt, E. Bordignon, D. Carbonera, J. P. Dekker, N. Karapetyan, C. Teutloff, A. Webber, W. Lubitz and E. Schlodder, *J. Biol. Chem.*, 2003, **278**, 46760–71.

43 P. Sétif, *Biochim. Biophys. Acta - Bioenerg.*, 2001, **1507**, 161–179.

44 N. Fischer, *EMBO J.*, 1998, **17**, 849–858.

45 K. Meimberg, N. Fischer, J.-D. Rochaix and U. Mühlenhoff, *Eur. J. Biochem.*, 1999, **263**, 137–144.

46 J. Noth, D. Krawietz, A. Hemschemeier and T. Happe, *J. Biol. Chem.*, 2013, **288**, 4368–4377.

47 O. Ben-Zvi, E. Dafni, Y. Feldman and I. Yacoby, *Biotechnol. Biofuels*, 2019, **12**, 266.

48 S. P. Chapman, C. M. Paget, G. N. Johnson and J.-M. Schwartz, *Front. Plant Sci.*, 2015, **6**, 474.

49 L. Wang, W. Gong, A. Lin and B. Hu, *Int. J. Biometeorol.*, 2014, **58**, 1711–1720.

50 D. L. Erbes, D. King and M. Gibbs, *Plant Physiol.*, 1979, **63**, 1138 LP – 1142.

51 R. C. Sicher, in *Advances in Photosynthesis Research: Proceedings of the VIth International Congress on Photosynthesis, Brussels, Belgium, August 1--6, 1983*, ed. C. Sybesma, Springer Netherlands, Dordrecht, 1984, pp. 413–416.

52 H. Takahashi, S. Clowez, F.-A. Wollman, O. Vallon and F. Rappaport, *Nat. Commun.*, 2013, **4**, 1954.

53 C. E. Lubner, a. M. Applegate, P. Knorzer, a. Ganago, D. a. Bryant, T. Happe and J. H. Golbeck, *Proc. Natl. Acad. Sci.*, 2011, **108**, 20988–20991.

54 S. Santabarbara, K. E. Redding and F. Rappaport, *Biochemistry*, 2009, **48**, 10457–10466.

55 H. BOHME, *Eur. J. Biochem.*, 1978, **83**, 137–141.

56 D. Weiß, G. Schneider, B. Niemann, P. Guttmann, D. Rudolph and G. Schmahl, *Ultramicroscopy*, 2000, **84**, 185–197.

57 J. E. W. Polle, J. R. Benemann, A. Tanaka and A. Melis, *Planta*, 2000, **211**, 335–344.